Geophysical Research Letters

RESEARCH LETTER
10.1029/2021GL094760

Response of the Low-Level Jet to Precession and Its Implications for Proxies of the Indian Monsoon

Chetankumar Jalihal[1,2,3], Jayaraman Srinivasan[2], and Arindam Chakraborty[1,2]

[1]Centre for Atmospheric and Oceanic Sciences, Indian Institute of Science, Bangalore, India, [2]DST-Centre of Excellence in Climate Change, Divecha Centre for Climate Change, Indian Institute of Science, Bangalore, India, [3]Now at Max Planck Institute for Meteorology, Hamburg, Germany

Key Points:

- Upwelling in the Arabian Sea in modern climate is closely linked to the strength of the low-level jet and the South Asian summer monsoon
- On longer timescales, along with the strength of the jet, the location as well as the width of the jet changes
- This affects the intensity and spatial extent of upwelling and has implications for the interpretation of proxies of upwelling

Supporting Information:

Supporting Information may be found in the online version of this article.

Correspondence to:

C. Jalihal,
jalihal@iisc.ac.in

Citation:

Jalihal, C., Srinivasan, J., & Chakraborty, A. (2022). Response of the low-level jet to precession and its implications for proxies of the Indian monsoon. *Geophysical Research Letters*, *49*, e2021GL094760. https://doi.org/10.1029/2021GL094760

Received 9 JUN 2021
Accepted 3 JAN 2022

Author Contributions:

Conceptualization: Jayaraman Srinivasan, Arindam Chakraborty
Formal analysis: Arindam Chakraborty
Investigation: Jayaraman Srinivasan, Arindam Chakraborty
Methodology: Jayaraman Srinivasan
Resources: Jayaraman Srinivasan, Arindam Chakraborty
Supervision: Jayaraman Srinivasan, Arindam Chakraborty
Validation: Jayaraman Srinivasan, Arindam Chakraborty
Writing – review & editing: Jayaraman Srinivasan

Abstract The long-term variations in the South Asian monsoon have been inferred based on the variations in the ocean productivity along the western coast of the Arabian Sea. The variations in ocean productivity were previously thought to be primarily influenced by the intensity of upwelling. Here, using idealized precession experiments in fully coupled climate models, we have shown that the area as well as the region of maximum upwelling change with precession. When summer occurs at perihelion (stronger summer insolation and monsoon precipitation), the area of upwelling is narrow. In contrast, during summer at aphelion (weaker summer insolation and monsoon precipitation), upwelling occurs over a broader region. This is due to the effect of convective heating over northeastern Africa and the western equatorial Indian Ocean on the width and meridional location of the low-level jet. Therefore, the upwelling inferred from proxies does not necessarily indicate the Indian summer monsoon strength.

Plain Language Summary Modern observations suggest that the upwelling along the western boundary of the Arabian Sea is primarily controlled by the strength of the low-level jet (LLJ). The strength of the LLJ and the Indian summer monsoon rainfall are also positively correlated. Hence, proxies of upwelling have been used to infer the variations in the monsoon of the distant past. We find, however, that factors other than the strength of the LLJ also affect upwelling. Variations in Earth's orbit alter the latitudinal location and width of the LLJ. This affects the area over which upwelling occurs and shifts the region of maximum upwelling. During periods of weaker summer insolation, the LLJ is broader and further south. This leads to an increase in the spatial extent of the upwelling. Therefore, the ocean productivity in the Arabian Sea is higher during such periods. This explains the large lag (~9 kyrs) with respect to the local summer insolation as observed in these proxies. Thus, we conclude that the proxies of upwelling capture multiple signals resulting from changes in the location, width, and strength of the LLJ and hence, are not appropriate for deducing the long-term variations in monsoon rainfall.

1. Introduction

The low-level jet (LLJ) in the Arabian Sea is a prominent feature of the Indian summer monsoon (Findlater, 1969, 1974; Halpern & Woiceshyn, 2001; Rajendran et al., 2012). The jet carries moisture from the Indian Ocean onto the Indian subcontinent. Thus, the strength of the LLJ is positively correlated with the Indian summer monsoon rainfall in the modern climate (Chakraborty et al., 2002, 2009; Joseph & Sijikumar, 2004). The upwelling induced along the western boundary of the Arabian Sea by the LLJ is proportional to the strength of the LLJ along the coast (coastal upwelling) and to the curl of wind stress (Ekman upwelling) offshore (Brock & McClain, 1992; Lee et al., 2000; Liao et al., 2016). It has been shown that stronger monsoons produce larger upwelling (Murtugudde et al., 2007). This relation has been used to reconstruct the strength of the past monsoons. Regions of upwelling are also regions of higher ocean productivity. Therefore, by measuring the productivity in these regions as archived in the sediment cores, upwelling can be inferred.

Evidence from such reconstructions indicates that the strength of upwelling lags local summer insolation by about 9 kyrs (Caley et al., 2011; Reichart et al., 1998; S. C. Clemens & Prell, 2003; S. C. Clemens et al., 2010; S. Clemens et al., 1991). Whether this can be interpreted as a lag in the South Asian monsoon has been a subject of debate (Gebregiorgis et al., 2020; Zhang et al., 2020) because several terrestrial proxies of monsoon suggest that monsoon rainfall is nearly in phase with local insolation (Zhang et al., 2019). Some studies have argued that the proxies of upwelling in the Arabian Sea are influenced by the location of the LLJ instead (Anderson &

Prell, 1992; Gupta et al., 2005; Le Mézo et al., 2017). Thus, indicating that the relationship between LLJ and the monsoon rainfall may be different in different climate regimes. This view is supported by recent studies where it was shown that it is the net energy flux into the atmosphere and water vapor, and not the monsoon winds that account for variability of South Asian monsoon on centennial and longer timescales (Jalihal, Srinivasan, et al., 2019; Jalihal et al., 2020).

The variations in precipitation over the Bay of Bengal are, however, linked to those in LLJ on precession timescales (Jalihal, Bosmans, et al., 2019; Jalihal et al., 2020). The LLJ extends into the Bay of Bengal and modulates the surface latent heat flux there. These fluctuations in the surface latent heat flux are large enough to counter the changes induced by insolation. Hence, precipitation over the Bay of Bengal is out-of-phase with local summer insolation. Thus, the orbital-scale variations in LLJ are linked to oceanic precipitation and not to the terrestrial precipitation within the South Asian monsoon domain.

The variations in the LLJ on intraseasonal and interannual timescales have been studied extensively (Arpe et al., 1998; Chen & van Loon, 1987; Fasullo & Webster, 2002; Halpern & Woiceshyn, 2001; Jain et al., 2021; Joseph & Sijikumar, 2004). Several studies have also highlighted that LLJ location and intensity are changing and are likely to change further due to global warming (Decastro et al., 2016; Preethi et al., 2017; Rajendran et al., 2012; Sandeep & Ajayamohan, 2015; Sandeep et al., 2018). A comprehensive study of LLJ variations on the orbital timescale is, however, missing. An understanding of the long-term variations in LLJ and the factors that drive it is necessary for the correct interpretation of the proxies. In this article, using fully coupled general circulation models, we have unraveled the factors that affect upwelling on the orbital timescale.

2. Data and Methods

We have used NCEP reanalysis over the period 1948–2017 to understand the connection between upwelling and precipitation at the interannual timescales. GPCP monthly precipitation data is used to evaluate precipitation over India. Reconstructions of upwelling from the Arabian Sea give an estimate of the upwelling on longer timescales. We have used several foraminifer assemblages from the cores RC27-61 (S. C. Clemens & Prell, 2003), MD04-2861 (Caley et al., 2011), and GeoB3004-1 (Schmiedl & Leuschner, 2005). The productivity estimates from the NIOP cores 455, 464, and 497 (Reichart et al., 1998) were also used. Furthermore, denitrification in the oxygen minimum zone also represents upwelling (Altabet et al., 2002; Reichart et al., 1998). Hence, we have used $\delta^{15}N$ from the cores RC27-14 and RC27-23 (Altabet et al., 2002). These proxies are spread across the western and northern Arabian Sea (Figure 1). Thus, they have the potential to provide an estimate of spatial variations in upwelling on longer timescales. Most of these records constitute the Arabian Sea monsoon stack by S. C. Clemens et al. (2010). At the precession mode, this stack is highly coherent with the orbital parameters as well as the $\delta^{18}O$ from caves in East Asia with a confidence level of 95%. These Arabian Sea upwelling records are compared with the $\delta^{18}O_{sw}$ ($\delta^{18}O$ of seawater; see methods in Jalihal, Srinivasan, et al., 2019 for a detailed description) from a sediment core near the mouth of Ganga-Brahmaputra in the northern part of the Bay of Bengal (Kudrass et al., 2001). Since this region is influenced by the run off from over land, this proxy captures the amount of terrestrial monsoon rainfall. The time sampling is not uniform across different proxies. Hence, we have interpolated all the proxies to an equally spaced interval of 500 years, following which a bandpass filter is applied to extract the precession modes (18–24 kyrs). For our analysis, we have considered the time period between 0 and 100 ka.

We have carried out time slice orbital experiments in the high resolution, fully coupled CESM 1.2.0 (Hurrell et al., 2013; Neale et al., 2012). The model consists of the CAM 5 (Community Atmospheric Model) for the atmospheric component and Parallel Ocean Program (POP) for the ocean model. CAM has a resolution of $0.9° \times 1.2°$, whereas the POP has a resolution of about 0.25° near the equator. The model was run with orbital configurations corresponding to the minimum and maximum precession (P_{min} and P_{max}), following the experimental setup used by Bosmans et al. (2015). In the precession minimum (P_{min}) orbital configuration, the boreal summer solstice occurs near the perihelion, whereas in the Precession maximum (P_{max}), it occurs at aphelion. The eccentricity is set close to the highest values that occurred in the last million years. This produces a difference in summer insolation (June-July-August) between P_{min} and P_{max}, over India of about 80 Wm^{-2} (Berger, 1978; Bosmans et al., 2015, 2018; Jalihal, Bosmans, et al., 2019). Each simulation is run for 100 years. Since precessional forcing modulates the seasonal cycle and does not affect the annual mean insolation, its impact on the intermediate and deep ocean can be assumed negligible. Thus, a simulation of 100 years is sufficient. The first 50 years

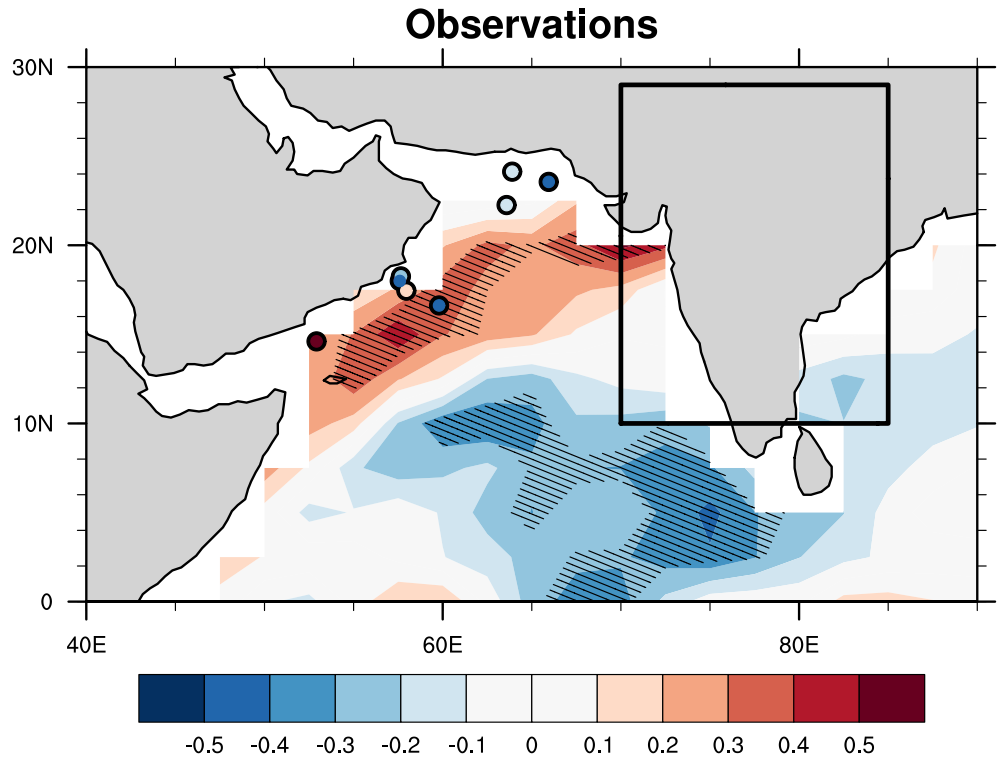

Figure 1. The spatial map of correlation between interannual June-July-August averaged rainfall over India and Ekman upwelling everywhere over the period 1948–2017. The inset black box represents the region over which area-averaged precipitation was evaluated (10°–29°N; 70°–85°E; land only grids). The hatched regions have significant correlation coefficients at the 90% confidence level. NCEP-reanalysis 1 data set was used to evaluate the curl of wind stress, and Global Precipitation Climatology Project data set was used for precipitation. The filled circles show the correlation between the proxy of the Indian monsoon, $\delta^{18}O_{sw}$ (Kudrass et al., 2001)and the proxies of upwelling in the Arabian Sea (Altabet et al., 2002; Caley et al., 2011; Reichart et al., 1998; S. C. Clemens & Prell, 2003; Schmiedl & Leuschner, 2005). These proxies were bandpass filtered for the precession modes (18–24 kyrs). The filled circles represent the location of the upwelling proxies. The color with which the circles are filled corresponds to the correlation of the proxy with that of the Indian monsoon proxy.

of the simulation are discarded as spin-up, and only the last 50 years are considered for the study. All the other boundary conditions are kept constant at their preindustrial values. The model has a decent representation of the climatological Indian summer monsoon (Figure S1 in Supporting Information S1). It has excess orographic precipitation along the foothills of the Himalayas. Compared to most CMIP5 models, CESM 1.2.0 has better climatological precipitation over India and reproduces the seasonal cycle quite well (Figures S2 and S3 in Supporting Information S1). To further validate our results, we have used data from the P_{min} and P_{max} simulations from another high-resolution fully coupled model: EC-Earth (Bosmans et al., 2015) and also from a transient simulation of climate over the last 22,000 years (TraCE-21K) with realistic forcings (Liu et al., 2009; He, 2011).

Modern observations and numerical simulations suggest that the high primary productivity in the western Arabian Sea is governed largely by two factors, viz. the coastal upwelling along the coast of Arabia and the offshore upwelling (Brock & McClain, 1992; Lee et al., 2000; Liao et al., 2016). The coastal upwelling is proportional to the wind stress (Sverdrup, 1951), whereas the offshore upwelling (Ekman upwelling) is determined by the curl of wind stress. Using simulations of productivity in the western Arabian Sea in a fully coupled climate model with an online biogeochemical model (Le Mézo et al., 2017) have shown that orbital forcing influences productivity in the western Arabian Sea through the Ekman upwelling. Hence, we have used Ekman upwelling in all our analyses, and it was evaluated as the curl of wind stress over the surface of the ocean:

$$W_e = \text{curl}\left(\frac{\tau}{\rho f}\right) \quad (1)$$

where, W_e is the upwelling averaged over the Ekman layer, ρ is the density of sea water (taken to be 1025 kg m^{-3}), f is the Coriolis parameter, τ is the wind stress on the surface of the ocean. τ is given by:

$$\tau = \rho_a * C_d * WS_{sfc} \quad (2)$$

ρ_a is the density of air (taken to be 1 kg m^{-3}), WS_{sfc} is the surface wind speed (10 m wind speed is used from NCEP and wind speed at 0.995 σ for model data). C_d is the drag coefficient and is given by Large and Pond (1981):

$$C_d = 0.001\,3 \qquad WS_{sfc} \leq 11 \ \text{m s}^{-1} \quad (3)$$

$$C_d = 10^{-3}(0.49 + 0.065 * WS_{sfc}) \qquad WS_{sfc} > 11 \ \text{m s}^{-1} \quad (4)$$

3. Results

3.1. Impact of Precession on the Relation Between the Arabian Sea Upwelling and South Asian Monsoon

Figure 1 depicts the correlation between the Indian summer monsoon rainfall (ISMR) and upwelling in the surrounding oceans at interannual timescales based on NCEP data. It shows that ISMR is positively correlated with upwelling in the northwestern Arabian Sea along the coast. Even though the reconstructions of upwelling lie within regions where upwelling is positively correlated with the ISMR, they register a negative correlation. This opposing correlation at the interannual and precession timescales (~23 kyrs) suggests that different processes link upwelling to the ISMR at different timescales. Moreover, the precession mode correlation is not spatially uniform. There are differences in the correlation as we move north. Near the Horn of Africa, it is positively correlated, but changes sign further north. Thus, suggesting a complex relationship between ISMR and upwelling on precession timescales.

Orbital forcing modulates both the ISMR as well as the LLJ (Jalihal, Bosmans, et al., 2019; Jalihal et al., 2020). Therefore, we have examined the relation between ISMR and upwelling due to variations in Earth's orbit (Figures 2a and 2b). We find that the relation between ISMR and upwelling is different under different climates (Figures 2a and 2b). During periods of high local summer insolation and climatological monsoon (P_{min}), the correlation between interannual variations in ISMR and upwelling is negligible. In contrast, during periods of weaker summer insolation and climatological monsoon (P_{max}), the correlation between interannual variations in ISMR and upwelling is stronger. Thus, underscoring that the relationship between ISMR and upwelling as seen in modern observations should not be extended for all climates.

The orbital configuration of P_{max} resembles the modern orbital configuration, albeit with higher eccentricity. The pattern of the correlation between ISMR and upwelling is, also similar (Figures 1 and 2b). The interannual variations in the latitude and strength of the LLJ is related to those in the gradient of surface pressure over the Arabian Sea (Chakraborty & Agrawal, 2017; Sandeep & Ajayamohan, 2015; Tomas & Webster, 1997; Webster et al., 2003). At the precession timescales, additional factors influence the location and strength of the LLJ (Jalihal, Bosmans, et al., 2019). Precipitation over northeastern Africa and the western equatorial Indian Ocean increase on account of higher summer insolation in P_{min} compared to P_{max} (Figure S4 in Supporting Information S1). The convective heating over these two regions drives a Matsuno-Gill-like response of the lower tropospheric winds (Jalihal, Bosmans, et al., 2019; Pausata et al., 2021). The ensuing Kelvin wave produces an anomalous easterly that leads to narrowing of the LLJ and also causes its maxima to shift northward (Jalihal, Bosmans, et al., 2019; Pausata et al., 2021). In the current study, we find a similar dependence at the interannual timescales as well in P_{min}. The interannual variations in precipitation over northeastern Africa and the western equatorial Indian Ocean have a greater impact on the LLJ, and hence on the upwelling in P_{min} (Figure 2c and Figure S5a in Supporting Information S1). In P_{max}, precipitation over these two regions is weaker. Therefore, they do not influence the upwelling in P_{max} at the interannual timescales (Figure 2d and Figure S5b in Supporting Information S1).

3.2. Change in Area of Upwelling

The proxies used to detect upwelling, in general, record the integrated effect of several years. Therefore, we next examine the climatology in our simulations. A change in precession leads to meridional shifts in the LLJ (Figures 3a and 3b). In P_{min}, the LLJ is parallel to the coast of Oman and is located in the northern Arabian Sea.

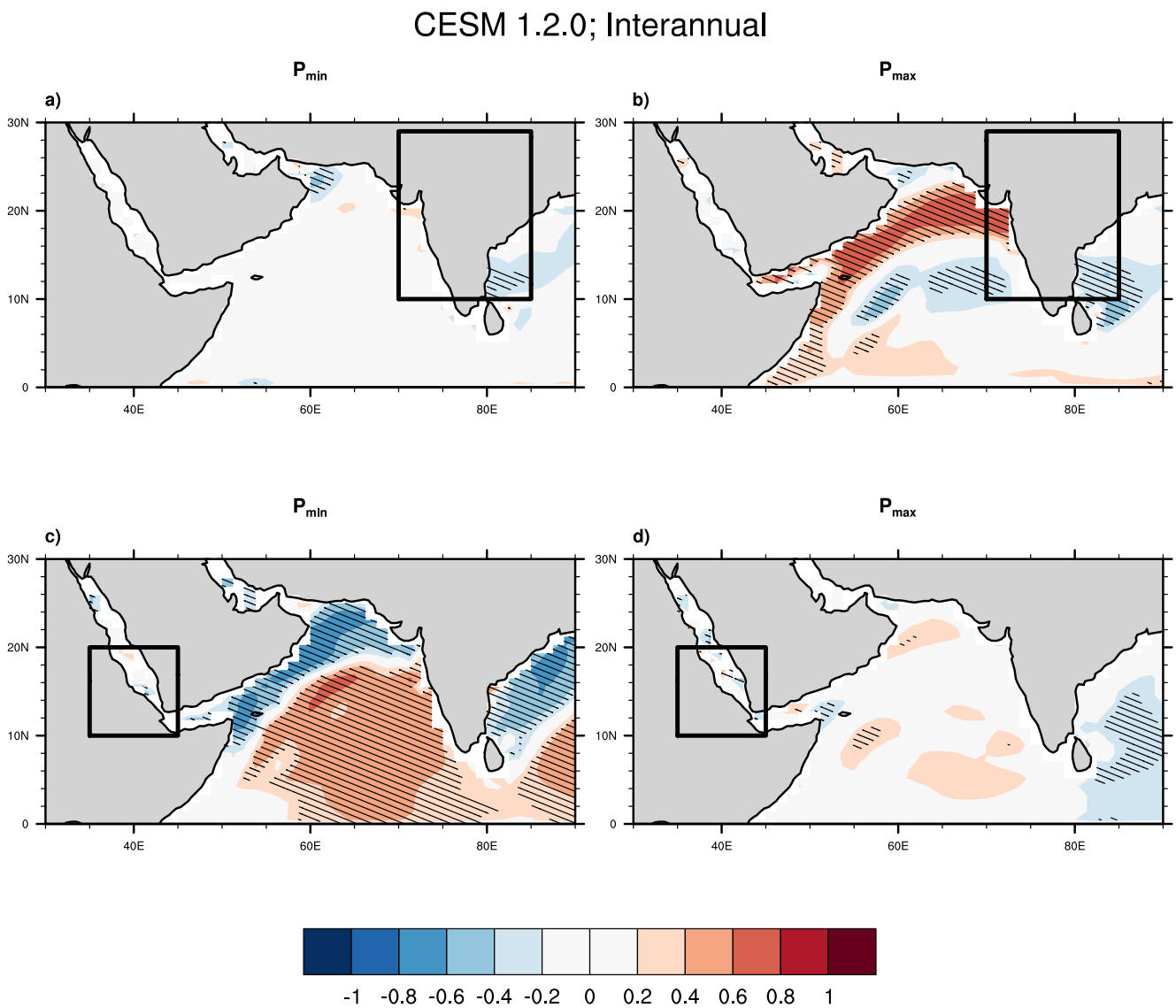

Figure 2. The spatial map of correlation between the June-July-August mean precipitation over the region represented by the inset boxes with Ekman upwelling over grids everywhere for the P_{min} simulation(a and c) and the P_{max} simulation(b and d). The area-averaged precipitation over the Indian monsoon region (10°–29°N; 70°–85°E; land only grids) is considered in (a and b), and over northeast Africa (10°–20°N; 35°–45°E) is taken in (c and d). The hatched regions have significant correlation coefficients at the 95% confidence level. The last 50 years of the simulation were used to generate the correlation maps.

The climatological summer monsoon is stronger in this experiment. On the other hand, summer insolation and ISMR are weaker in P_{max}. The LLJ is further south as compared to its location in P_{min}. Along with this southward shift, the strength of the LLJ also changes. The maximum velocity is higher in P_{max} and is located near the Horn of Africa. There is a change in the width of the LLJ as well. The LLJ is broader in P_{max} and is narrower in P_{min} (Figures 3a and 3b). Thus, suggesting that the orbital scale variability of the LLJ consists of fluctuations in the strength, meridional location, and width, whereas, its interannual fluctuations are primarily due to changes in its strength (Figure S6 in Supporting Information S1). The variations in the strength, magnitude, and location of the LLJ on precession timescales are due to the additional influence of convective heating over northeastern Africa and the western equatorial Indian Ocean (Jalihal, Bosmans, et al., 2019; Pausata et al., 2021; Figure S4 in Supporting Information S1).

Since upwelling is determined by the curl of wind stress, any changes in the location, width, or strength of the LLJ would have an impact on upwelling. Therefore, we have compared the curl of wind stress from the two experiments to understand the impact of the changes in the LLJ (Figure 4). In P_{min} (stronger summer insolation),

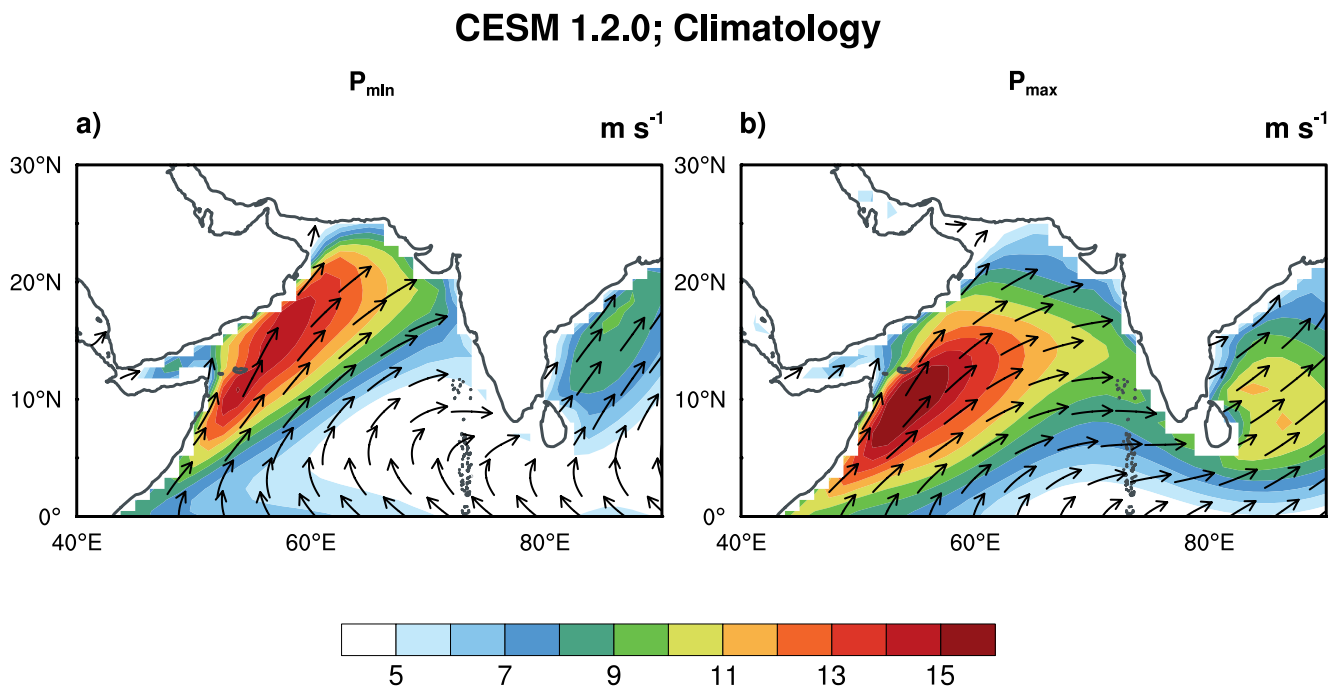

Figure 3. The June-July-August averaged climatological surface wind speed in shading for (a) P_{min} (strong monsoon) and (b) P_{max} (weak monsoon). The unit vectors indicate the direction of surface winds.

upwelling is concentrated along the western boundary of the Arabian Sea and extends all the way into the northern parts of the Arabian Sea. In P_{max}, the intensity of upwelling increases along the Horn of Africa. This region of largest upwelling extends up to 15°N. The upwelled water gets advected along with the nutrients to the northern Arabian Sea (Caley et al., 2011). Therefore, most of the proxies would capture a stronger signal in climates with P_{max}–like orbital configurations. Furthermore, the area over which upwelling occurs in the northern Arabian Sea more than doubles in P_{max}. This explains why most of the proxies suggest a large lag with respect to the local summer insolation. Such changes in the area of upwelling are not observed on interannual timescales (Figure S7

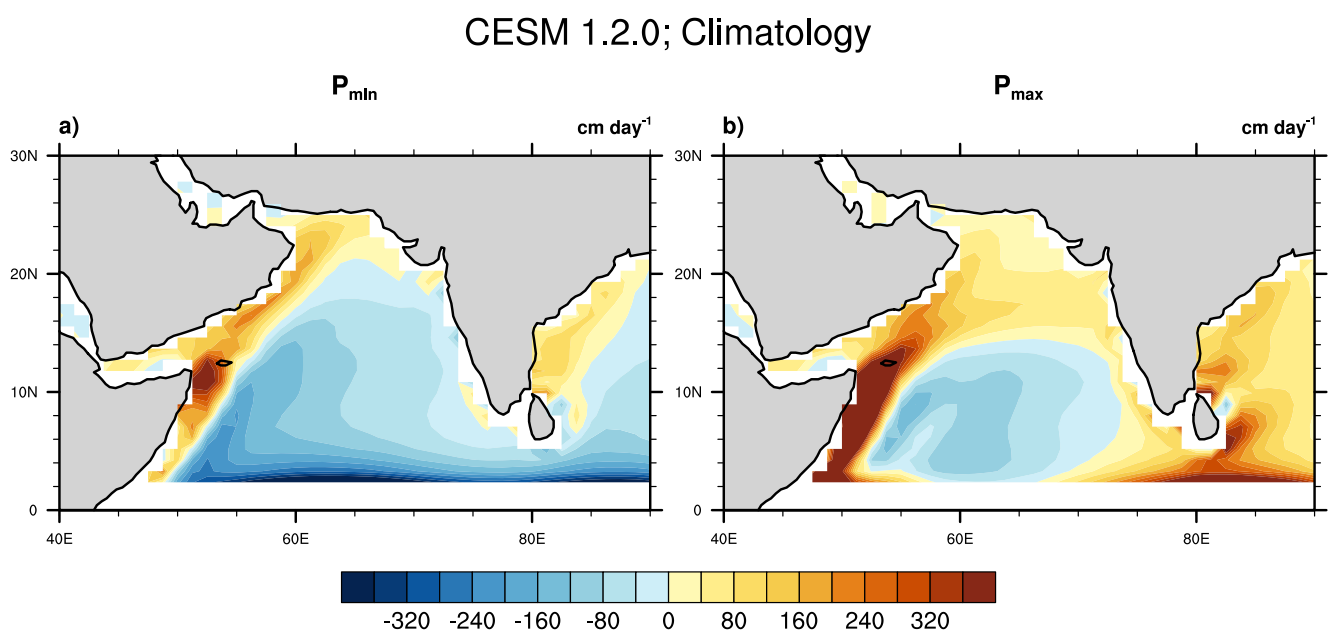

Figure 4. The June-July-August averaged climatological Ekman upwelling in shading for the climate for (a) P_{min} (strong monsoon) and (b) P_{max} (weak monsoon).

in Supporting Information S1). These results are consistent in P_{min} and P_{max} simulations using another fully coupled model- EC-Earth (Figure S8 in Supporting Information S1). The out-of-phase relation between upwelling and ISMR can also be seen in TraCE-21k (Figure S9 in Supporting Information S1). The Indian monsoon is weak at the last glacial maximum, and it strengthens across the deglacial, reaches a maximum around early Holocene (~10 ka), and gradually weakens during the Holocene. Contrarily, Ekman upwelling is strongest at the last glacial maximum. It decreases across the deglacial to reach a minimum at around the early Holocene and increases in strength through the Holocene.

4. Discussion and Conclusions

Different proxies have been used to reconstruct the long-term variations in the monsoon. Some of the proxies, in particular, the $\delta^{18}O$ from caves, indicate that monsoon is nearly in phase with local summer insolation (Cheng et al., 2012; Zhang et al., 2019). Reconstructions of upwelling along the western coast of the Arabian Sea, which was previously believed to be proportional to monsoon strength, suggests that upwelling (and hence monsoon) lags local summer insolation significantly at the precession mode. A comprehensive mechanism for the cause of lag in the proxies from the Arabian Sea was still missing. Furthermore, the previous studies did not explain the diverging relation between the Indian monsoon rainfall and upwelling at interannual and precession modes.

In this study, we have demonstrated that along with the changes in wind speed of the LLJ, the changes in the width of the jet, and its meridional location influence upwelling in the Arabian Sea. On interannual timescales, the changes in the wind speed govern the seasonal mean upwelling (Figure S6 in Supporting Information S1). At the precession timescales, the variations in the width and latitude of the jet also play a crucial role. These are influenced by convective heating in the western equatorial Indian Ocean and northeastern Africa (Jalihal, Bosmans, et al., 2019; Jalihal et al., 2020). These convective heat sources are a result of precessional forcing. The changes in the strength, width, and latitude of the LLJ are such that the curl of wind stress is stronger during climates with weaker summer insolation. Moreover, the spatial extent of upwelling is substantially larger. Thus, proxies register enhanced productivity (upwelling) in such climates even though the summer monsoon is weaker. Another high-resolution fully coupled climate model shows consistent results. Similar result from a transient simulation of climate over the last 22,000 years (TraCE-21k) with realistic forcings in a fully coupled CCSM4 further enhances confidence in our results (Figure S9 in Supporting Information S1). Thus, upwelling-based proxies do not represent the variability of the South Asian monsoon at the precession mode. This also explains the large lag observed between upwelling and other terrestrial proxies of the monsoon. The proxies of upwelling were previously thought to represent the South Asian monsoon and were found to have a large lag with respect to the terrestrial proxies, sparking off a long-standing debate (Caley et al., 2011; Gebregiorgis et al., 2020; Wang et al., 2014; Zhang et al., 2019, 2020). Our results show that upwelling-based proxies in the Arabian Sea are not linked to the Indian monsoon rainfall at precession timescales.

Recent reconstructions of the monsoon spanning multiple glacial-interglacial cycles suggest a stronger influence of changes in greenhouse gas concentrations and ice volume (Beck et al., 2018; Maher & Thompson, 2012; McGrath et al., 2021; S. C. Clemens et al., 2021; S. Clemens et al., 2018). This is in direct contrast to some of the speleothem reconstructions from East Asia, which suggest changes in insolation predominantly drive monsoons. In our previous work (Jalihal, Srinivasan, et al., 2019; Jalihal et al., 2020), using the energetics of monsoons we have shown in the TraCE-21k that net energy flux into the atmosphere (Q_{div}) and total column water vapor (P_{wat}) are enough to explain the orbital scale variability of monsoons. Insolation drives fluctuations in monsoons primarily through Q_{div}, whereas greenhouse gases and ice sheets affect the gross moist stability through their impact on P_{wat}. Thus, the impact of other forcings is accounted for. In these studies, we had used a domain that covers most of the South Asian monsoon region. The relative impact of these forcings might vary from one region to another. This could be one reason why some of the proxies suggest a stronger influence of forcings other than insolation. Moreover, since the simulation used in these studies is only 22 Kyrs long, the relative role of insolation and other forcings on monsoons on the glacial-interglacial timescales cannot be determined fully. Greenhouse gas and ice sheet forcings also affect the LLJ and hence the curl of wind stress (Le Mézo et al., 2017). This could be a reason why proxies of upwelling indicate a lag of 5–9 Kyrs with local summer insolation instead of the 12 Kyrs lag (Precession maximum and minimum are separated by 12 Kyrs). Additionally, other processes such as lateral advection of coastally upwelled nutrients due to alongshore wind stress, the transport of nutrients by mesoscale eddies and filaments, vertical mixing, and mixed layer depth could also affect the lag in the proxies.

Fertilization of the upper ocean by dust can also impact primary productivity (Liao et al., 2016; Wiggert & Murtugudde, 2007). During periods of weaker monsoons, dust emission is higher due to an increase in the area of the arid regions. This is another factor that could be the reason for the opposite phase of primary productivity with insolation. Furthermore, it has also been argued that the timing of the supply of nutrients to the euphotic zone is influenced by the Atlantic Meridional Overturning Circulation (AMOC; Ziegler et al., 2010). The changes in the relative impact of these processes in response to orbital, greenhouse gas, and ice-sheet forcings might lead to the spatially nonuniform relation between proxies of upwelling and the Indian monsoon (Figure 1). High-resolution eddy-resolving ocean models are required to understand the impact of changes in these processes on primary productivity in response to glacial-interglacial forcings.

Proxy reconstructions are based on the relation between physical processes observed in the modern climate. Our results underscore that additional factors can impact the interpretation of some of the proxies on longer timescales. For example, since the region of upwelling expands and shrinks out-of-phase with the strength of the Indian monsoon on precession timescales, the upwelling signal captured by the proxy in many cases is out-of-phase with the Indian monsoon.

Data Availability Statement

The CESM 1.2.0 data used in this study is available at https://doi.org/10.5281/zenodo.5140156. The NCEP reanalysis data was obtained from https://psl.noaa.gov/data/gridded/data.ncep.reanalysis.html. The GPCP precipitation data is publicly available at https://psl.noaa.gov/data/gridded/data.gpcp.html. The $\delta^{18}O$ from the sediment core KL-126 (Kudrass et al., 2001) was obtained from https://doi.pangaea.de/10.1594/PANGAEA.735053. Data from the cores RC27-14 and RC27-23 (Altabet et al., 2002) can be accessed from https://www.ncdc.noaa.gov/paleo-search/study/2617. The data from NIOP497, NIOP464, and NIOP455 cores (Reichart et al., 1998) is available at https://www.ncdc.noaa.gov/paleo-search/study/2557. The data from the core RC27-61 (S. C. Clemens & Prell, 2003) can be accessed from https://www.ncdc.noaa.gov/paleo-search/study/5882. We are thankful to T. Caley for providing the data from the core MD04-2861 (Caley et al., 2011). Data from the core GeoB3004-1 is available at https://doi.pangaea.de/10.1594/PANGAEA.738202. The EC-Earth data used here can be accessed from https://doi.org/10.5281/zenodo.5054419. The TraCE-21k data set, can be downloaded from the Earth System Grid (National Center for Atmospheric Research) https://www.earthsystemgrid.org/project/trace.html.

Acknowledgments
We thank S.C. Clemens and K. Thirumalai for their comments. This work has benefitted from discussion with P.N. Vinayachandran and D. Shankar. We thank Supercomputer Education and Research Centre (SERC), Indian Institute of Science, Bangalore, for making available the computation facilities to carry out the simulations. The authors acknowledge support from the Centre for Excellence in the Divecha Centre for Climate Change (DCCC), supported by the Department of Science and Technology, Government of India. C.J. is grateful to DCCC for financial assistance.

References

Altabet, M. A., Higginson, M. J., & Murray, D. W. (2002). The effect of millennial-scale changes in Arabian Sea denitrification on atmospheric CO_2. *Nature*, *415*(6868), 159–162. https://doi.org/10.1038/415159a

Anderson, D. M., & Prell, W. L. (1992). The structure of the southwest monsoon winds over the Arabian Sea during the late quaternary: Observations, simulations, and marine geologic evidence. *Journal of Geophysical Research*, *97*(C10), 15481–15487. https://doi.org/10.1029/92jc01428

Arpe, K., Dümenil, L., & Giorgetta, M. A. (1998). Variability of the Indian monsoon in the ECHAM3 model: Sensitivity to sea surface temperature, soil moisture, and the stratospheric quasi-biennial oscillation. *Journal of Climate*, *11*(8), 1837–1858. https://doi.org/10.1175/1520-0442-11.8.1837

Beck, J. W., Zhou, W., Li, C., Wu, Z., White, L., Xian, F., & An, Z. (2018). A 550,000-year record of East Asian monsoon rainfall from ^{10}Be in loess. *Science*, *360*(6391), 877–881. https://doi.org/10.1126/science.aam5825

Berger, A. (1978). Long-term variations of daily insolation and quaternary climatic changes. *Journal of the Atmospheric Sciences*, *35*(12), 2362–2367. https://doi.org/10.1175/1520-0469(1978)035<2362:ltvodi>2.0.co;2

Bosmans, J., Erb, M., Dolan, A., Drijfhout, S., Tuenter, E., Hilgen, F., & Lourens, L. (2018). Response of the Asian summer monsoons to idealized precession and obliquity forcing in a set of GCMs. *Quaternary Science Reviews*, *188*, 121–135. https://doi.org/10.1016/j.quascirev.2018.03.025

Brock, J. C., & McClain, C. R. (1992). Interannual variability in phytoplankton blooms observed in the northwestern Arabian sea during the southwest monsoon. *Journal of Geophysical Research*, *97*(C1), 733–750. https://doi.org/10.1029/91jc02225

Caley, T., Malaizé, B., Zaragosi, S., Rossignol, L., Bourget, J., Eynaud, F., et al. (2011). New Arabian Sea records help decipher orbital timing of Indo-Asian monsoon. *Earth and Planetary Science Letters*, *308*(3–4), 433–444. https://doi.org/10.1016/j.epsl.2011.06.019

Chakraborty, A., & Agrawal, S. (2017). Role of west Asian surface pressure in summer monsoon onset over central India. *Environmental Research Letters*, *12*, 074002. https://doi.org/10.1088/1748-9326/aa76ca

Chakraborty, A., Nanjundiah, R., & Srinivasan, J. (2002). Role of Asian and African orography in Indian summer monsoon. *Geophysical Research Letters*, *29*(20), 50–51. https://doi.org/10.1029/2002gl015522

Chakraborty, A., Nanjundiah, R. S., & Srinivasan, J. (2009). Impact of African orography and the Indian summer monsoon on the low-level Somali jet. *International Journal of Climatology: A Journal of the Royal Meteorological Society*, *29*(7), 983–992. https://doi.org/10.1002/joc.1720

Chen, T. C., & van Loon, H. (1987). Interannual variation of the tropical easterly jet. *Monthly Weather Review*, *115*(8), 1739–1759. https://doi.org/10.1175/1520-0493(1987)115<1739:ivotte>2.0.co;2

Cheng, H., Sinha, A., Wang, X., Cruz, F. W., & Edwards, R. L. (2012). The global paleomonsoon as seen through speleothem records from Asia and the Americas. *Climate Dynamics*, *39*(5), 1045–1062. https://doi.org/10.1007/s00382-012-1363-7

Clemens, S., Holbourn, A., Kubota, Y., Lee, K., Liu, Z., Chen, G., & Fox-Kemper, B. (2018). Precession-band variance missing from East Asian monsoon runoff. *Nature Communications*, *9*(1), 1–12. https://doi.org/10.1038/s41467-018-05814-0

Clemens, S., Prell, W., Murray, D., Shimmield, G., & Weedon, G. (1991). Forcing mechanisms of the Indian Ocean monsoon. *Nature*, *353*(6346), 720–725. https://doi.org/10.1038/353720a0

Clemens, S. C., & Prell, W. L. (2003). A 350,000 year summer-monsoon multi-proxy stack from the Owen Ridge, northern Arabian Sea. *Marine Geology*, *201*(1–3), 35–51. https://doi.org/10.1016/s0025-3227(03)00207-x

Clemens, S. C., Prell, W. L., & Sun, Y. (2010). Orbital-scale timing and mechanisms driving late Pleistocene Indo-Asian summer monsoons: Reinterpreting cave speleothem δ^{18}O. *Paleoceanography*, *25*, PA4207. https://doi.org/10.1029/2010pa001926

Clemens, S. C., Yamamoto, M., Thirumalai, K., Giosan, L., Richey, J. N., Nilsson-Kerr, K., & McGrath, S. M. (2021). Remote and local drivers of Pleistocene South Asian summer monsoon precipitation: A test for future predictions. *Science Advances*, *7*, eabg3848. https://doi.org/10.1126/sciadv.abg3848

Decastro, M., Sousa, M., Santos, F., Dias, J., & Gómez-Gesteira, M. (2016). How will Somali coastal upwelling evolve under future warming scenarios? *Scientific Reports*, *6*(1), 1–9. https://doi.org/10.1038/srep30137

Fasullo, J., & Webster, P. (2002). Hydrological signatures relating the Asian summer monsoon and ENSO. *Journal of Climate*, *15*(21), 3082–3095. https://doi.org/10.1175/1520-0442(2002)015<3082:hsrtas>2.0.co;2

Findlater, J. (1969). A major low-level air current near the Indian Ocean during the northern summer. *Quarterly Journal of the Royal Meteorological Society*, *95*(404), 362–380. https://doi.org/10.1002/qj.49709540409

Findlater, J. (1974). The low-level cross-equatorial air current of the western Indian Ocean during the northern summer. *Weather*, *29*(11), 411–416. https://doi.org/10.1002/j.1477-8696.1974.tb04329.x

Gebregiorgis, D., Clemens, S. C., Hathorne, E. C., Giosan, L., Thirumalai, K., & Frank, M. (2020). A brief commentary on the interpretation of Chinese speleothem δ^{18}O records as summer monsoon intensity tracers. *Quaternary*, *3*(1), 7. https://doi.org/10.3390/quat3010007

Gupta, A. K., Das, M., & Anderson, D. M. (2005). Solar influence on the Indian summer monsoon during the Holocene. *Geophysical Research Letters*, *32*, L17703. https://doi.org/10.1029/2005gl022685

Halpern, D., & Woiceshyn, P. M. (2001). Somali jet in the Arabian Sea, El Niño, and India rainfall. *Journal of Climate*, *14*(3), 434–441. https://doi.org/10.1175/1520-0442(2001)014<0434:sjitas>2.0.co;2

He, F. (2011). Simulating transient climate evolution of the last deglaciation with CCSM3 (PhD dissertation). University of Wisconsin.

Hurrell, J. W., Holland, M. M., Gent, P. R., Ghan, S., Kay, J. E., Kushner, P. J., et al. (2013). The community earth system model: A framework for collaborative research. *Bulletin of the American Meteorological Society*, *94*(9), 1339–1360. https://doi.org/10.1175/bams-d-12-00121.1

Jain, S., Mishra, S. K., Anand, A., Salunke, P., & Fasullo, J. T. (2021). Historical and projected low-frequency variability in the Somali jet and Indian summer monsoon. *Climate Dynamics*, *56*(3), 749–765. https://doi.org/10.1007/s00382-020-05492-z

Jalihal, C., Bosmans, J. H. C., Srinivasan, J., & Chakraborty, A. (2019). The response of tropical precipitation to Earth's precession: The role of energy fluxes and vertical stability. *Climate of the Past*, *15*, 449–462. https://doi.org/10.5194/cp-15-449-2019

Jalihal, C., Srinivasan, J., & Chakraborty, A. (2019). Modulation of Indian monsoon by water vapor and cloud feedback over the past 22,000 years. *Nature Communications*, *10*(5701), 1–8. https://doi.org/10.1038/s41467-019-13754-6

Jalihal, C., Srinivasan, J., & Chakraborty, A. (2020). Different precipitation response over land and ocean to orbital and greenhouse gas forcing. *Scientific Reports*, *10*(11891), 1–11. https://doi.org/10.1038/s41598-020-68346-y

Joseph, P., & Sijikumar, S. (2004). Intraseasonal variability of the low-level jet stream of the Asian summer monsoon. *Journal of Climate*, *17*(7), 1449–1458. https://doi.org/10.1175/1520-0442(2004)017<1449:ivotlj>2.0.co;2

Kudrass, H., Hofmann, A., Doose, H., Emeis, K., & Erlenkeuser, H. (2001). Modulation and amplification of climatic changes in the northern hemisphere by the Indian summer monsoon during the past 80 ky. *Geology*, *29*(1), 63–66. https://doi.org/10.1130/0091-7613(2001)029<0063:maaocc>2.0.co;2

Large, W., & Pond, S. (1981). Open ocean momentum flux measurements in moderate to strong winds. *Journal of Physical Oceanography*, *11*(3), 324–336. https://doi.org/10.1175/1520-0485(1981)011<0324:oomfmi>2.0.co;2

Le Mézo, P., Beaufort, L., Bopp, L., Braconnot, P., & Kageyama, M. (2017). From monsoon to marine productivity in the Arabian Sea: Insights from glacial and interglacial climates. *Climate of the Past*, *13*(7), 759–778. https://doi.org/10.5194/cp-13-759-2017

Lee, C. M., Jones, B. H., Brink, K. H., & Fischer, A. S. (2000). The upper-ocean response to monsoonal forcing in the Arabian Sea: Seasonal and spatial variability. *Deep Sea Research Part II: Topical Studies in Oceanography*, *47*(7–8), 1177–1226. https://doi.org/10.1016/s0967-0645(99)00141-1

Liao, X., Zhan, H., & Du, Y. (2016). Potential new production in two upwelling regions of the western Arabian Sea: Estimation and comparison. *Journal of Geophysical Research: Oceans*, *121*(7), 4487–4502. https://doi.org/10.1002/2016jc011707

Liu, Z., Otto-Bliesner, B., He, F., Brady, E., Tomas, R., & Clark, P. (2009). Transient simulation of last deglaciation with a new mechanism for Bølling-Allerød warming. *Science*, *325*(5938), 310–314. https://doi.org/10.1126/science.1171041

Maher, B. A., & Thompson, R. (2012). Oxygen isotopes from Chinese caves: Records not of monsoon rainfall but of circulation regime. *Journal of Quaternary Science*, *27*(6), 615–624. https://doi.org/10.1002/jqs.2553

McGrath, S. M., Clemens, S. C., Huang, Y., & Yamamoto, M. (2021). Greenhouse gas and ice volume drive Pleistocene Indian summer monsoon precipitation isotope variability. *Geophysical Research Letters*, *48*, e2020GL092249. https://doi.org/10.1029/2020gl092249

Murtugudde, R., Seager, R., & Thoppil, P. (2007). Arabian Sea response to monsoon variations. *Paleoceanography*, *22*, PA4217. https://doi.org/10.1029/2007pa001467

Neale, R. B., Chen, C. C., Gettelman, A., Lauritzen, P. H., Park, S., Williamson, D. L., et al. (2012). Description of the NCAR community atmosphere model (CAM 5.0). *NCAR Tech. Note NCAR/TN-486+ STR*, *1*(1), 1–12.

Pausata, F. S. R., Messori, G., Yun, J., Jalihal, C. A., Bollasina, M. A., & Marchitto, T. M. (2021). The remote response of the south Asian monsoon to reduced dust emissions and Sahara greening during the middle Holocene. *Climate of the Past*, *17*, 1243–1271. https://doi.org/10.5194/cp-17-1243-2021

Preethi, B., Mujumdar, M., Kripalani, R., Prabhu, A., & Krishnan, R. (2017). Recent trends and tele-connections among south and East Asian summer monsoons in a warming environment. *Climate Dynamics*, *48*(7–8), 2489–2505. https://doi.org/10.1007/s00382-016-3218-0

Rajendran, K., Kitoh, A., Srinivasan, J., Mizuta, R., & Krishnan, R. (2012). Monsoon circulation interaction with Western Ghats orography under changing climate. *Theoretical and Applied Climatology*, *110*(4), 555–571. https://doi.org/10.1007/s00704-012-0690-2

Reichart, G. J., Lourens, L., & Zachariasse, W. (1998). Temporal variability in the northern Arabian Sea oxygen minimum zone (OMZ) during the last 225,000 years. *Paleoceanography*, *13*(6), 607–621. https://doi.org/10.1029/98pa02203

Sandeep, S., & Ajayamohan, R. (2015). Poleward shift in Indian summer monsoon low level Jetstream under global warming. *Climate Dynamics*, *45*(1–2), 337–351. https://doi.org/10.1007/s00382-014-2261-y

Sandeep, S., Ajayamohan, R., Boos, W. R., Sabin, T., & Praveen, V. (2018). Decline and poleward shift in Indian summer monsoon synoptic activity in a warming climate. *Proceedings of the National Academy of Sciences*, *115*(11), 2681–2686. https://doi.org/10.1073/pnas.1709031115

Schmiedl, G., & Leuschner, D. C. (2005). Oxygenation changes in the deep western Arabian Sea during the last 190,000 years: Productivity versus deepwater circulation. *Paleoceanography*, *20*, PA2008. https://doi.org/10.1029/2004pa001044

Sverdrup, H. U. (1951). Evaporation from the oceans. In *Compendium of meteorology* (pp. 1071–1081). Springer. https://doi.org/10.1007/978-1-940033-70-9_86

Tomas, R. A., & Webster, P. J. (1997). The role of inertial instability in determining the location and strength of near-equatorial convection. *Quarterly Journal of the Royal Meteorological Society*, *123*(542), 1445–1482. https://doi.org/10.1002/qj.49712354202

Wang, P., Wang, B., Cheng, H., Fasullo, J., Guo, Z., Kiefer, T., & Liu, Z. (2014). The global monsoon across timescales: Coherent variability of regional monsoons. *Climate of the Past*, *10*(6), 2007–2052. https://doi.org/10.5194/cp-10-2007-2014

Webster, P., Magana, V., Palmer, T. (2003). Dynamical theory. *Encyclopedia of Atmospheric Sciences* (pp. 1370–1385).

Wiggert, J. D., & Murtugudde, R. G. (2007). The sensitivity of the southwest monsoon phytoplankton bloom to variations in Aeolian iron deposition over the Arabian Sea. *Journal of Geophysical Research*, *112*, C05005. https://doi.org/10.1029/2006jc003514

Zhang, H., Ait Brahim, Y., Li, H., Zhao, J., Kathayat, G., & Tian, Y. (2019). The Asian summer monsoon: Teleconnections and forcing mechanisms—A review from Chinese speleothem $\delta^{18}O$ records. *Quaternary*, *2*(3), 26. https://doi.org/10.3390/quat2030026

Zhang, H., Cheng, H., Baker, J., & Kathayat, G. (2020). Response to comments by Daniel Gebregiorgis et al. "A brief commentary on the interpretation of Chinese speleothem $\delta^{18}O$ records as summer monsoon intensity tracers". *Quaternary*, *3*(1), 8. https://doi.org/10.3390/quat3010008

Ziegler, M., Lourens, L. J., Tuenter, E., Hilgen, F., Reichart, G.-J., & Weber, N. (2010). Precession phasing offset between Indian summer monsoon and Arabian Sea productivity linked to changes in Atlantic overturning circulation. *Paleoceanography*, *25*, PA3213. https://doi.org/10.1029/2009pa001884

Reference From the Supporting Information

Bosmans, J., Drijfhout, S., Tuenter, E., Hilgen, F., & Lourens, L. (2015). Response of the North African summer monsoon to precession and obliquity forcings in the EC-Earth GSM. *Climate Dynamics*, *44*(1–2), 279–297.